JOURNAL OF SPACECRAFT AND ROCKETS
Vol. 45, No. 4, July–August 2008

Method for Crew-Escape Risk-Envelope Assessment During Ascent

Christopher J. Freitas* and Ryan M. Keedy†
Southwest Research Institute, San Antonio, Texas 78238-5166

DOI: 10.2514/1.33753

Computational simulations and analyses may be used to quantify the risk envelope for crew escape resulting from an accidental detonation of explosive materials at a specified time during the ascent phase for crew exploration vehicles. Here, a methodology was developed and applied to assess the explosive risk potential, focusing on internal detonations or explosions. The approach was to computationally model the geometry of a launch vehicle and the time evolution of an accident scenario with explosive detonation. A series of detailed detonation simulations were completed for three different crew exploration vehicle launch vehicle configurations. All simulations assumed the formation of an explosive mixture of liquid oxygen and liquid hydrogen. Two different energy-release models were used in this study. One was based on programmed burn with a Jones–Wilkins–Lee analytical description of the reaction-product expansion isentrope, and the other used a volumetric energy source formulation. Based on this methodology and simulations, the predicted pressure field had significant magnitudes in the region of the service module and crew exploration vehicle. In fact, the overpressure is so severe that it would not be a survivable event for the crew.

Nomenclature

S = fragment size or effective diameter, m or in.
K = material fracture toughness, MPa · $m^{0.5}$ or ksi · $in.^{0.5}$
ρ = material density, kg/m^3 or $lbm/in.^3$
c = material speed of sound, m/s or in./s
ε = strain rate, s^{-1}
w = explosive charge or mixture weight, N or lb

I. Introduction

NASA is concerned with the hazard posed to flight crews by accidental failure of propulsion systems resulting in an internal or external detonation or explosion. A crew-escape risk-envelope assessment is required to quantify the hazard posed to flight crews that are due to explosions or detonations. An internal detonation or explosion refers to the accidental release and mixing of fuel and oxidizer within the body of the launch vehicle, resulting in a multiphase explosive mixture that subsequently detonates. For cryogenic propellants such as liquid hydrogen (LH_2) and liquid oxygen (LOX), this multiphase mixture may consist of liquid phases, hydrogen gas, and LOX crystals. An external detonation or explosion then refers to the accidental release of fuel and oxidizer such that mixing and detonation occurs externally to the vehicle. An explosive-hazard potential is also posed by failure of solid-propellant propulsion systems (solid rocket motors) after their scheduled initiation. A distinction is made here between a detonation and an explosion, in which the near-field overpressure magnitude defines the difference between an explosion (which is characterized by a reduced near-field overpressure) and a detonation (which exhibits a larger near-field overpressure). The overpressure magnitudes for a detonation vs an explosion generally differ by an order of magnitude. This concept is discussed in greater detail in Sec. III of this paper.

Crew-escape risk-envelope assessments define the parameter space for the conditions that a crew may experience either during an accident scenario or during escape operations that are due to an accident scenario. The objective of this study was then to provide a quantification of this risk envelope for crew escape resulting from an accidental detonation of explosive materials at a specified time during the ascent phase for a launch vehicle system. This study focused only on internal detonations or explosions. To assess the crew-escape risk envelope for these types of explosive hazards during the ascent phase, a computational methodology was developed to simulate and predict the magnitude of the explosive-hazard environment in the region of the crew module. The four variables that describe the hazard environment due to detonation or explosion are the overpressure field, the velocity field due to the propagating blast wave, the thermal environment (radiation and convection), and the fragment field resulting from material and structural failure. Blast overpressure may be characterized by peak pressure (measured in pascals) and/or specific-impulse–time histories (integration of the pressure–time-history curve in pascal seconds). In this study, peak pressure is used to characterize the blast overpressure. Similarly, the thermal environment may be characterized by peak temperature or heat flux to a surface (essentially, the integral of the temperature–time history over a surface). The fragment field is characterized by fragment size (or mass) and velocity of fragments.

The approach taken in this study to evaluate the crew-escape risk envelope was based on the use of existing computational codes to model the geometry of a launch vehicle and the time evolution of an accident scenario and explosive detonation. Through the analysis of the predicted pressure, velocity, temperature, and fragment fields, insights into the performance requirements for sizing of abort motor systems may be obtained. In this study, the two dominant explosive-environment parameters in terms of crew survivability are the local peak reflected overpressure off of the crew exploration vehicle (CEV) (measured in pascals) and the fragment field in the region of the CEV. Peak reflected overpressure is the appropriate metric for the assessment of blast damage. For many structures, including the human body, peak overpressure values have been established or correlated to different damage states or magnitudes for the structure [1]. For example, overpressures in the range of 69 to 83 kPa will result in destruction of most buildings, and an overpressure in the range of 250 to 5000 kPa is lethal to the human body. The lethal range in peak overpressure for humans is inversely proportional to the pulse duration: the shorter the pulse duration, the greater the peak pressure must be to be lethal. For example, to achieve 100% lethality, a peak overpressure in the range of 1100–1500 kPa need be applied for 3 ms [2].

Received 27 July 2007; revision received 4 March 2008; accepted for publication 6 March 2008.

*Senior Program Manager, Computational Mechanics.
†Research Engineer, Computational Mechanics.

Fragment fields are also a critical evaluation parameter in this context, due to the penetration capability of the fragments and the collateral damage to the vehicle that will result. Thermal effects may also be a critical parameter, but are generally considered to be of greater importance in on-pad accidents, in which a parachute may be deployed shortly after jettison of the crew module and may be directly in the line of sight to a fireball. For ascent-phase accidents, in which a parachute is not deployed until late in the crew-escape elapsed-time interval, fireball temperature is not an important parameter, due to the dissipation of the detonation thermal field by the time of parachute deployment. This study therefore focused on peak overpressure and fragment-field characteristics in the region of the crew module (or CEV) for the launch vehicle systems analyzed in assessing the risk envelope.

This paper provides the details of the analysis approach, including discussions on the code used in the simulations, the modeling of explosions/detonations, the launch vehicle model conditions and geometries, and the fragmentation model employed. Key results are presented and discussed.

II. Computational Methods

The computational code used to simulate the detonation or explosion of the LOX/LH_2 mixtures and the collateral damage to the launch vehicle is CTH. CTH is an Eulerian shock-physics wave-propagation code [3] and represents a class of computer codes called hydrocodes. An introduction to the fundamentals of hydrocodes is given by Wilkins [4]. CTH (not an acronym) is developed and maintained at Sandia National Laboratories, and has the capability to model dynamic events that include explosive detonation and high-velocity impact. The CTH code solves the differential equations describing conservation of mass, momentum, and energy during transient dynamic events on a fixed spatial mesh (thus the Eulerian reference). In fact, CTH uses a Lagrangian advection step that is then remapped to the original grid system, resulting in an Eulerian formulation at the end of the time step. CTH is capable of tracking the interactions of up to 20 materials using different formulations for interface reconstruction, ranging from first-order to second-order formulations. This code contains models suitable to describe material response under most conditions encountered in shock physics, including penetration, failure, sympathetic explosive response, and explosive energy release. Material response consists of an equation of state for the mean stress, a plasticity model for the deviatoric stresses, and a fracture model to insert a void into the grid system when the tensile stress has been exceeded. CTH also provides the ability to predict fragment formation and characteristics.

A variety of materials and material-insert geometries are available to facilitate the modeling of complex structures and geometries. The structural elements are inserted into the physical domain as a sequence of solid objects, with the ability to delete subcomponents of the objects permitting the construction of hollow structures, for example. The computational mesh is Cartesian (rectangular, cylindrical, or spherical coordinates) and is not tied to the structure (as it is for Lagrangian formulations), and thus changes in numerical resolution are easily accommodated.

The Eulerian formulation of the code permits large deformations without computational penalty, as in Lagrangian formulations, and allows for multimaterials in computational cells to develop as appropriate for explosive or impact events. However, this requires that sufficient grid resolution be maintained so that material interfaces within a computational cell are accurately defined. To support efficient fine-grid simulations, CTH also incorporates an adaptive mesh refinement scheme, that based on user-specified criteria, will track high gradient regions through dynamic refinement of the grid system. In the fragment analysis simulations performed in this study, the adaptive mesh refinement method was used to track the aluminum skin of the vehicle and fuel/oxidizer tanks.

Recently, CTH was put through a verification and validation exercise for condensed-phase (solid explosives) detonations in enclosures. Based on direct comparison with full-scale experimental data, CTH predicted pressure–time histories and impulse–time histories with a minimum of 87% accuracy [5]. The features of CTH relevant to this study are the prediction of blast overpressure, structural material failure, and formation of fragments. For additional information on CTH, the reader is directed to [3].

III. Explosion Versus Detonation Modeling

Mixtures of hydrogen gas and air or oxygen gas can be detonated under some mixture conditions. Hydrogen forms flammable mixtures at ambient temperatures and pressures with oxygen, air, chlorine, and oxides of nitrogen. It forms these mixtures in the gas or vapor phase. In propulsion systems, hydrogen is a cryogenic fuel stored as a liquid (as well as oxygen) at extremely low temperatures (20 K for LH_2 and 90 K for LOX). Hydrogen must then undergo a change of phase to achieve a flammable mixture with the oxidizer. The rate at which liquid hydrogen changes phase is dictated by the dynamics of the release process and the ability of heat to be transferred to the liquid phase. In general, the temperature of the liquid must be increased above the vaporization temperature or boiling point of the liquid (flash temperature). Heat is transferred to the liquid by conduction only if the liquid is static and by convection and conduction if the liquid is moving at some velocity. In the accident scenarios evaluated in this study, the hydrogen and oxygen are released at the common bulkhead separating the LH_2 and LOX tanks. For this condition, a mixture is formed consisting of liquid phases, cold hydrogen vapor, and oxygen crystals (which have formed due to contact with the colder LH_2). Typically at atmospheric conditions, the flammable limits for a hydrogen-vapor–air mixture are 4 and 75% by volume, and for a hydrogen-vapor–oxygen mixture are 4 and 95% by volume, both at 25°C and atmospheric pressure. These limits for hydrogen mixtures typically define the lowest and highest concentrations for which the mixtures will combust or burn; mixtures with concentrations less than or greater than these limits will not burn. However, experimental data [6] suggest that autoignition of liquid-phase mixtures of LH_2 and LOX, such as in the scenario studied here, is likely. The possible mechanism for autoignition of the liquid mixtures is a piezoelectric effect (crystals that acquire a charge when placed under stress) due to the interaction of the frozen LOX crystals and cold hydrogen vapor, but this has yet to be confirmed. Because of the potential for autoignition, it is likely that the explosive mixture volume will tend to be small; however, to date, no experimental or computational data can provide an estimate for the volume of the mixture sufficient for an explosion or detonation. Thus, in this effort, the volumes of the explosive mixtures simulated were selected to bound the range of volumes believed to develop, based on limited data from past accidents.

When a flammable mixture is heated to an elevated temperature by an ignition source (which includes autoignition by a piezoelectric effect), a reaction is initiated that may proceed with sufficient speed to ignite the mixture to a self-sustaining condition. Typically, there is a time lag between the instant that the ignition source begins to elevate the local temperature of the mixture and when the mixture combusts, and this time lag is a function of the strength of the ignition source. Once the mixture is ignited and the resulting flame is self-sustaining, the flame will either attach itself to the ignition source or propagate through the mixture. If the propagation speed is subsonic (based on the unburned mixture properties), then a deflagration results, and if the propagation speed of the flame front is supersonic, then the mixture has detonated. In the case of a deflagration, the flame-front propagation is slow enough to allow for pressure equalization to occur across the front, and thus the overpressure due to a deflagration tends to be small (overpressure ratios up to 10:1 [7]). However, in the case of a detonation, insufficient time is available to achieve pressure equilibrium across the flame front, allowing for the pressure shock front to detach from the flame front. The flame front lags behind the shock front sufficiently to allow it to achieve local pressure equilibrium. The result is that the overpressure due to a detonation is significant with overpressure ratios of up to 45:1 [7]. Finally, a deflagration may transition to a detonation, but is dependent on the mixture, temperature, pressure, ignition source, and geometry.

As already discussed, mixtures of hydrogen and oxygen can be detonated given the appropriate mixture conditions and strength of ignition source (measure in joules). In addition, ideal-gas Chapman–Jouget theory and chemical-thermoequilibrium-based solutions indicate that LOX/LH_2 gas-phase mixtures can detonate. However, there is also considerable evidence that suggests that in the accident scenarios discussed here, a true detonation is unlikely, although very high rates (an explosion) of energy release are likely and have been observed from ground-based tests. Figure 1 (taken from [6]) demonstrates the broad range of peak incident-pressure data measured for hydrogen detonations and explosions in ground-based tests. Scaled distance in this figure is the distance from the geometry center of the charge or mixture to a measurement location (measured in feet or meters) divided by the charge weight w to the third power (measured in pounds or newtons). The data in the near-field region (in particular, at a scaled distance less than three) exhibits a large amount of scatter, or variability. However, there is also a trend to this region, which suggests a near-field response of a reduced magnitude when compared with a condensed-phase detonation such as TNT. The curve fit through the data captures two key observations. First, below a scaled distance of 3 $ft/w^{1/3}$ (1.5 $m/N^{1/3}$), the incident pressure in the hydrogen/oxygen explosion is significantly less than that generated by detonation of a condensed-phase explosive [trinitrotoluene (TNT)]. Second, at scaled distance greater than 3 $ft/w^{1/3}$, there is little distinction between a detonation and the explosion; that is, in the near field, the TNT curve is observed to continue to much larger pressures, rather than rolling off to a relatively constant and lower pressure magnitude as with the hydrogen–oxygen mixtures.

CTH has several different models for describing detonations and explosions. The two relevant models to this analysis are the high-explosive-burn or programmed-burn explosive model with a Jones–Wilkins–Lee (JWL) analytical description of the reaction-product expansion isentrope as defined in [4] and the volumetric energy source model. In the programmed-burn model, the time at which the detonation wave arrives at any given location in the explosive material is defined as the line-of-sight distance from a user-specified ignition point to the specific location divided by the detonation velocity. The energy is released locally per computational cell containing explosive material over a few computational cycles, when the simulated time coincides with the predetermined detonation time for the cell. The explosive products then expand from the Chapman–Jouget pressure state. The shock front in the explosive travels at the prescribed detonation velocity and all of the explosive material is assumed to detonate. This model is the typical approach used when simulating condensed explosives or explosive materials that have large rates of energy release over short time intervals.

The volumetric-energy-source model allows the user to specify a region of the computational domain from which internal energy can be deposited over a specified elapsed time interval. In this model, the user specifies a material type, the total magnitude of energy inserted with that material, the rate of energy insertion, the time duration of the insertion, and the spatial region in which the material is to accept the energy. This model allows for specification of significantly longer time intervals for release of explosive energy than that provided by the programmed-burn model. In fact, the programmed-burn model cannot reproduce the near-field trend of the explosive energy release from a LOX/LH_2 mixture, as seen in Fig. 1, for any set of input parameters. This is due to the short time interval for energy release in the programmed-burn model. The time period of energy release (rate of energy release) is the critical parameter when trying to predict the near-field response of a LOX/LH_2 mixture explosion. However, the volumetric energy source model can reproduce the near-field response of a LOX/LH_2 mixture explosion. This is demonstrated in Fig. 2.

Figure 2 displays results from CTH simulations for a charge mass of 2595 kg detonating or exploding in a standard atmosphere as a free expansion (incident-pressure magnitude) using a programmed-burn model (results identified as TNT in Fig. 2) and the volumetric source model (explosion). In the programmed-burn model formulation, the LOX/LH_2 mixture is converted into an equivalent TNT charge with a standard JWL coefficient set. The volumetric source model uses a mixture density of 0.0056 g/cm^3 and energy per unit mass of 4.4 kJ/g. The time interval for release of this energy per unit mass is then specified as either 5, 10, or 20 ms. The incident pressure is then plotted as a function of scaled distance ($ft/w^{1/3}$). As reference, the gas-phase explosion curve fit of Fig. 1 is also displayed in Fig. 2 (as LH_2 data). In general, as the time interval for energy release becomes longer, the near-field pressure approaches the experimental data values, and then for still longer time intervals of energy release, the pressure magnitude falls below the experimental data. In addition, differences in pressures in the near field are reduced as the scaled distance is increased, and all distinction between the different models is finally lost.

In the simulations performed in this study, the volumetric burn model is used with the following parameter values: 10-ms release time interval, energy content of 4.4 kJ/g, and mixture mass-averaged density of 1.106 g/cm^3. These values were selected based on the analysis performed for Fig. 2 and result in a slightly conservative prediction (greater than the measured data) of overpressure magnitude for LOX/LH_2 mixtures, experimental data which include gas- and liquid-mixture explosions. We also used the programmed-burn model in this study. When used, the mixture mass is converted to an equivalent TNT charge mass and a standard set of TNT JWL coefficients are specified.

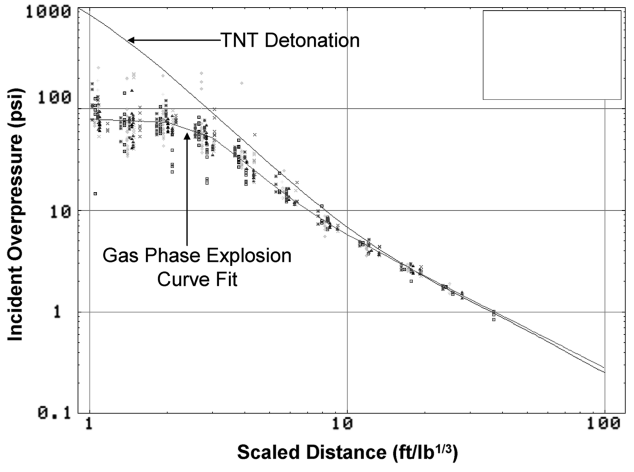

Fig. 1 Pressure vs scaled distance for hydrogen explosions/detonations [6].

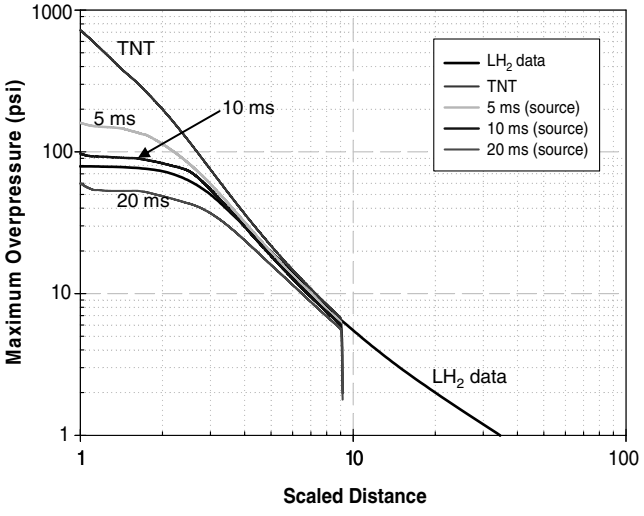

Fig. 2 Pressure vs scaled distance for different explosion models.

IV. Fragmentation Modeling

Under loading conditions in which materials undergo expansion strain rates (tensile stress), it has been found that the characteristic dimension of the fragments that form can be determined by the strain rate at the time of fracture. Grady [8] derived the basic relationships between strain rate and fragment dimensions that result as materials fracture under high-strain-rate loading conditions. Grady's model for fragment size is defined as

$$S = \left(\frac{4.89K}{\rho c \varepsilon}\right)^{2/3}$$

where S is the average fragment size (defined by a characteristic length scale), K is the material fracture toughness, ρ is the material density, c is the material's speed of sound, and ε is the strain rate. In this analysis, the temperature and strain-rate regimes are such that fragmentation is governed by the fracture toughness K of the structural materials.

Fragment characteristics (size or length scale and velocity) are evaluated in these simulations, but do not couple back into the calculation to form discrete fragments [9]. As material is driven into expansion by the explosive overpressure, the divergent motion (tensile load) induces a strain rate that is then used to calculate S. In the current application, overpressures will accelerate regions of the vehicle structures, and local monitoring (using tracer points) of the strain rates for expansion is used to estimate the average fragment size. The fragment dimension calculated by the preceding relationship is, as stated, an average. It is well documented that even under uniform strain rate, material will break into a distribution of fragment sizes (see [9]). A Poisson distribution provides one method for describing the scatter about the mean size. However, in this analysis, only the average fragment size is reported. Because of the few materials present in the launch vehicle structure (aluminum and core material) and the uniformity of the structure of the launch vehicle under load, it is believed that the size distribution of fragments will also be more uniform (with a small distribution around the mean), and thus the average fragment size is deemed to be the best measure in this analysis.

The preceding methodology [9], commonly referred to as the Grady–Kipp method, is based on predicting the strain rate that develops in the material at the time of failure. To determine the time of failure in the simulation, the minimum principal stress is used. When the minimum principal stress in the material achieves a relatively constant negative value (or the maximum local tensile stress of the material has been achieved), then computationally, failure of the material has occurred. CTH then begins to insert a void into the failed computational cells, and the local stress is released or relieved and returns to a zero value; thereby, locally, the structure can carry no further loads. The local time of failure has now been established, and based on that time, the local strain rate is determined and then applied to calculate the fragment size.

This methodology is then implemented here using the following steps:

1) Lagrangian tracers are specified and are attached to structural materials in the simulation.

2) The time-dependent position of each tracer is then tracked during the simulation.

3) The minimum principle stress is monitored at the tracer locations to determine the time of material failure.

4) The strain-rate–time history is also monitored at the tracer location because, as already indicated, the strain rates at or during the time of failure dictate the fragment size.

5) The velocity–time history is also monitored at the tracer locations, and at the time of failure, it sets the magnitude of the fragment velocity.

6) Using the data at each tracer location and the model for S, we are able to predict fragment size, fragment mass, and fragment velocity.

To illustrate this procedure, we present the following example. A generic second-stage booster is defined in which a 3633-kg TNT charge mass is detonated. Figure 3 shows the geometry for this

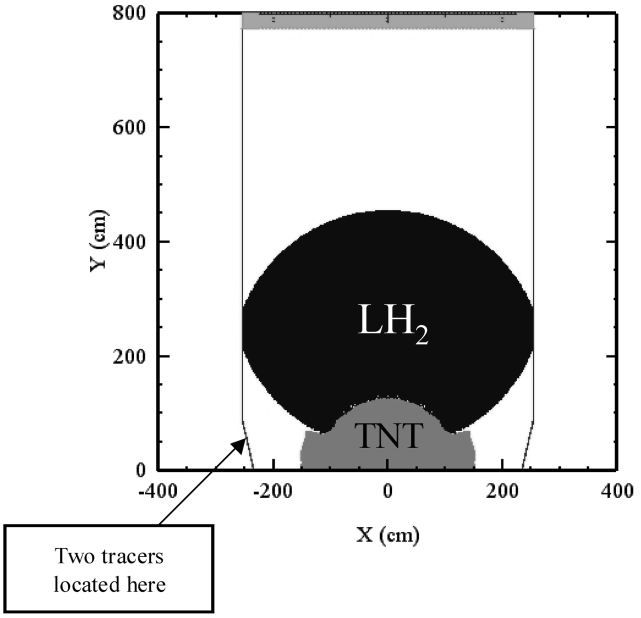

Fig. 3 Geometry of a generic second-stage booster.

demonstration, in which an explosive mixture has formed immediately below the LH_2 tank and has been cast into an equivalent TNT charge mass and simulated using programmed burn (in the figure, the charge mass has detonated and is expanding). The walls of the launch vehicle are modeled as 7075 aluminum with an adjusted wall thickness to account for the aluminum and core material. Details of this formulation are presented in [10]. Two Lagrangian tracers are embedded in the aluminum wall, as indicated in Fig. 3.

The predicted time histories for minimum principle stress, strain rate, and material velocity at the tracer locations are displayed in Fig. 4. This simulation had a grid resolution sufficient to resolve the 0.91-cm-thick wall with approximately nine zones. The minimum-principal-stress–time histories indicate that failure is initiated at approximately 0.8 ms for tracer 1 and at approximately 1 ms for tracer 2. We know that failure has occurred at these locations, because the stress had achieved a maximum tensile stress that is then followed by a period of stress relief or decrease to a zero stress value, due to failure of the material in the computational cell. The time of failure is generally taken to be the time after which a maximum tensile stress has been achieved and maintained. During the period of relatively constant tensile stress magnitude, the computational method is inserting a void into the computational cell, and upon completion of void insertion, the stress is relieved and returns to zero. The corresponding strain rates are then bounded by values of 750 and 1500 s^{-1}. Using the preceding fragment model and the predicted tracer data, the average fragment size or diameter then ranges from 2.6 to 4.1 cm. In general, the greater the strain rate, the smaller the fragment size. The corresponding fragment velocities then range from 1300 to 500 m/s.

V. Launch Vehicle Configurations and Simulations

Three different launch vehicle configurations were studied. The configurations were designated as EELV2, ILC_RSRB 4, and CLV-4. Complete details of these three configurations are presented in [10]. However, briefly, the EELV2 configuration consisted of a first stage with three LOX/rocket-propellant motors and a second-stage LOX/LH_2 booster. The ILC_RSRB and CLV-4 were similar in configuration and each had a first-stage solid rocket motor and a second-stage LOX/LH_2 booster. Different liquid-fuel loads were used in each configuration (see Table 1) as well as different ascent-phase profiles. For all configurations the same CEV and service module (SM) were used and are displayed in Fig. 5.

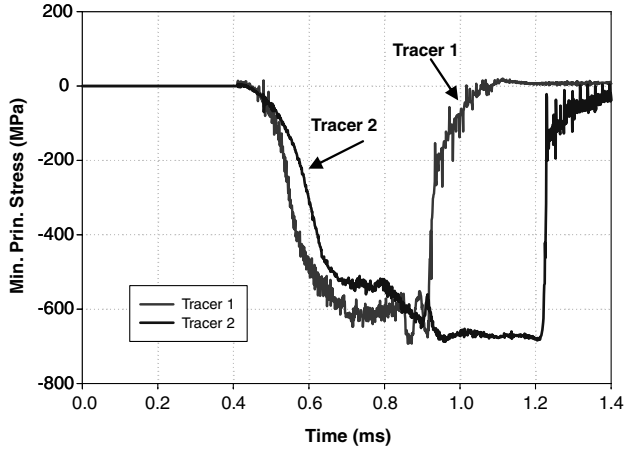

a)

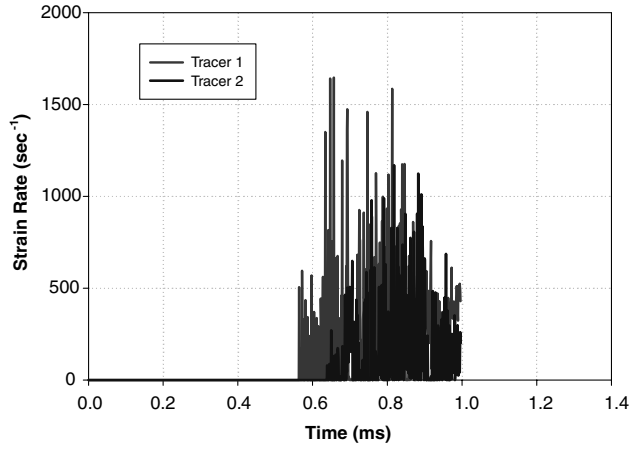

b)

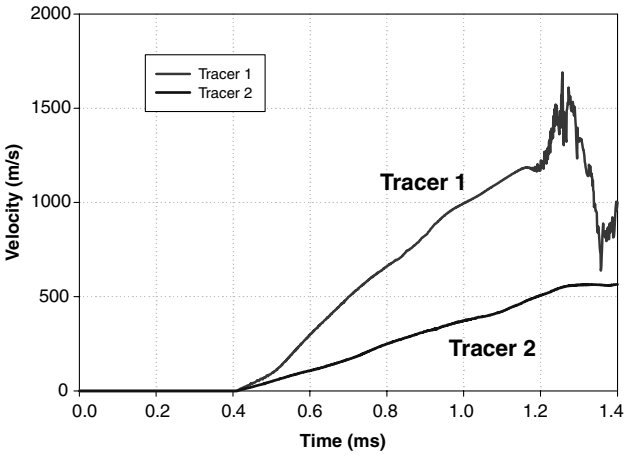

c)

Fig. 4 Time histories of data at tracer locations.

The basic accident scenario simulated for all configurations was a failure in the second-stage-booster propulsion system. It was assumed that a common bulkhead configuration of the LH_2 and LOX tanks existed (in the EELV2 configuration, there is a small gap between the tanks). A common bulkhead configuration is one in which the LOX and LH_2 tanks share a common bulkhead, in which the LH_2 tank generally sits above the LOX tank and the bulkhead defines, respectively, the bottom or top surface of the tanks. Given that configuration, with an LH_2 tank sitting on top of a LOX tank, the failure scenario has a rupture in the common bulkhead forming and resulting in direct contact and mixing of cryogenic LH_2 and LOX. This mixture then undergoes a phase change, forming an explosive gas-phase mixture that fills the available open space in the region of the common bulkhead. It is assumed that the mixture forms stoichiometrically with a mixture ratio of 5.5:1 for oxygen:hydrogen (which is the stoichiometric ratio for oxygen and hydrogen mixtures). A stoichiometric mixture of oxygen and hydrogen represents the worst-case condition, with the potential for maximum energy release and blast overpressure. Different charge masses are simulated with the masses being a percentage of the total fuel load on the vehicle. The charge mass is assumed to be spherical. Table 1 provides a summary of the range of charge masses simulated in this effort.

Table 1 Definition of charge masses simulated

Configuration	Fuel load, kg		Charge mass, kg			
	LH_2	LOX	1%	6%	10%	14%
EELV2	3993	21,959	260	1557	2595	3633
ILC_RSRB 4	15,907	87,486	1034	6204	10,339	N/A
CLV-4	25,140	138,270	1634	9805	16,341	N/A

The general definition for each group of simulations performed is illustrated in Figs. 6–8, in which the geometry and layout for the EELV2, ILC_RSRB 4, and CLV-4 second-stage boosters are displayed with a 10% charge mass. The CLV-4 configuration included more than just the second-stage booster: it also included the solid rocket motor, due to the time at which the accident scenario occurred. In all configurations and simulations, the CEV and SM remained attached to the second-stage booster. All simulations are axisymmetric.

For each vehicle configuration, a different set of initial conditions was defined. These selected conditions were deemed by the design community to be the most critical for each configuration. For the EELV2 configuration, the simulated event occurs at a mission elapsed time (MET) of 350 s. At MET the vehicle is at an altitude of

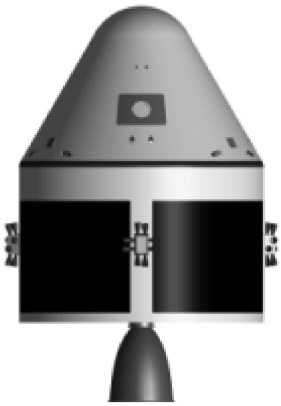

Fig. 5 CEV and SM.

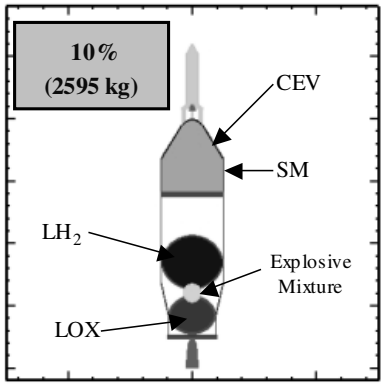

Fig. 6 EELV2 configuration and initial conditions.

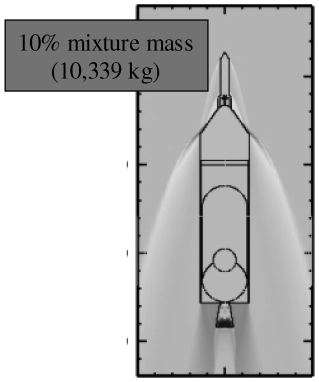

Fig. 7 ILC_RSRB 4 configuration and initial conditions.

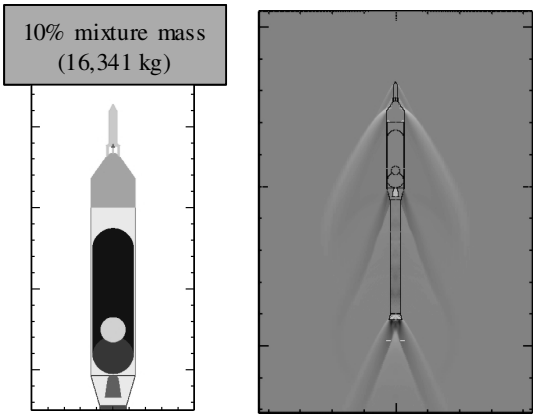

Fig. 8 CLV-4 configuration and initial conditions.

375,000 ft and moving with a speed of 5.3 km/s. At this altitude, the atmosphere is negligible and was neglected in the simulations. For the ILC_RSRB 4 vehicle, the MET is 125 s, which corresponds to an altitude of 180,000 ft and vehicle speed of 2.1 km/s. At this altitude, the atmosphere has an ambient pressure of 40 Pa, density of $5.4e-07$ g/cm^3, and a temperature of 259.5 K. The atmosphere was included in these simulations and an additional 50 ms of simulated time was required for the pressure field to achieve a steady state before detonation. For the CLV-4 configuration, the MET is only 50 s and corresponds to vehicle Max Q. At this time, the solid rocket motors are engaged and providing maximum thrust, and so they are still attached to the second stage and were thus included in the simulations. At this time, the CLV-4 vehicle is relatively low in the Earth's atmosphere, with an altitude of 30,000 ft and a speed of 762 m/s. The ambient atmosphere has a pressure of 30,103 Pa (4.4 psia), density of $4.6e-04$ g/cm^3, and temperature of 229 K. The atmosphere was also included in these simulations, with an additional 60 ms of simulated time being required for the pressure field to achieve a steady state before detonation.

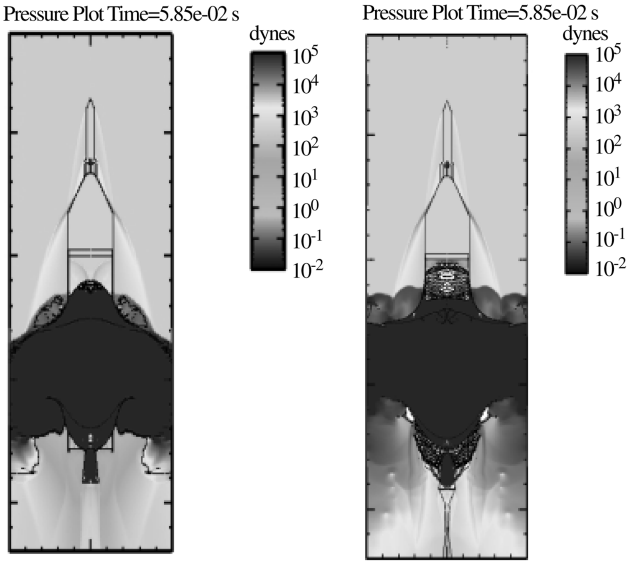

Fig. 9 Characteristics of near-field environment for an ILC_RRB 4 configuration with 10% charge mass; volumetric source model (left) and programmed burn (right); simulated time is approximately 58 ms for each image.

In each of the simulation series, both approaches to modeling the explosion are applied; that is, a simulation with programmed burn using an equivalent TNT charge mass was applied and a volumetric source was applied for many of the charge masses. In general, the programmed-burn simulations resulted in a more intense near-field response of the residual liquid propellants, resulting in the breakup of the fluid volume into droplets. For the volumetric source model, because the release of energy is significantly slower, the residual fuel tended to remain coherent and respond as a continuous fluid layer. The consequence of this was that the volumetric source model resulted in larger overpressures on the aft end of the SM. This was due to a hydrodynamic ram effect and the tradeoff of droplet/air-mixture density for liquid density only. Figure 9 displays these near-field characteristics.

Table 2 summarizes the peak reflected pressures as predicted in the volumetric source simulations. In that table, the aft-end SM refers to tracer points along the aft end of the SM and along the side of the SM and the side of the CEV. The side CEV tracers are along the sloped surface of the CEV. Both the incident-pressure pulse and the reflected-pressure pulse reflecting off of the SM and CEV are recorded at these tracer locations. Although the pressures tend to be low (and survivable) along the side of the SM and CEV, they clearly are not low (nor survivable) along the aft end of the SM. These loads would overwhelm the SM structure and result in significant loading of the aft end of the CEV. In these simulations, the SM and CEV are

Table 2 Summary of peak reflected pressure

Configuration	Charge mass, %	Peak reflected Pressure (psia)			
		Aft-end SM	Side SM	Side CEV	Aft-end SM (free expansion)
EELV2	1	1450	1	<1	30
	6	29,006	1.5	<1	50
	10	43,511	3	<1	80
	14	36,259	11	<1	80
ILC_RSRB 4	1	44	1	1	30
	6	1595	1	1	70
	10	2031	1	1	80
CLV 4	1	73	10	1	25
	6	4641	61	1.5	60
	10	8992	2320	46	80

modeled as a single solid material, because the details of the internals for these components were not yet defined. This modeling approach has no significance to the predicted overpressure. The conclusion to be drawn from these simulations is that if the CEV remains attached to the SM and second-stage booster and an explosive accident occurs, the loading of the SM (and, subsequently, the CEV) is so severe that it would not be a survivable event. Finally, in Table 2, the last column represents the incident overpressure as represented by the gas-phase explosive curve fit of Fig. 1 and for the distances from the center of the charge to the aft end of the SM for each configuration (and accounting for each charge mass). This column of data should be compared with the corresponding aft-end SM column (column 3). The difference in magnitude between these two columns is due to incident-vs-reflected pressure, the effect of residual fuel, and focusing of the blast by vehicle geometry.

The fragment sizes that result from these pressure-loading histories range in size from 15 to 90 cm and have velocities ranging from 800 to 25 m/s. The programmed-burn simulation predicted an additional class of fragments that were smaller and with significantly greater velocity: specifically, a size of 2 to 6 cm with a velocity of 1800 to 1300 m/s. To evaluate the lethality of these fragment sizes, a series of penetration simulations were performed in which candidate fragments moving at an appropriate velocity were impacted on a 2.54-cm-thick aluminum plate (a plate thickness representative of the aggregate launch vehicle wall thickness). For all fragment sizes and velocities simulated, the fragments perforated the aluminum plate. Complete details of this analysis are given in [10].

VI. Conclusions

A series of detailed explosion and detonation simulations were completed for three different launch vehicle configurations. All simulations assumed the formation of a gas-phase explosive mixture of LOX/LH_2. This mixture formed either at the region between the LH_2 or LOX tanks or at the common bulkhead shared by the tanks. The charge mass was on the centerline of the vehicle. Two different energy-release models were used: one based on programmed burn with a JWL analytical description of the reaction-product expansion isentrope and the other using a volumetric energy source formulation. These models predicted similar but different amplitude-pressure–time histories. These differences were the result of the programmed-burn model predicting larger near-field pressures that fragmented the residual liquid fuel into droplets that subsequently reduced peak reflected pressures. The volumetric source model, due to a slower release of energy and validated by experimental data, did not fragment the residual fuel, but rather transported it as a coherent fluid layer. This fluid layer then resulted in larger peak reflected pressures.

The predicted pressure field in all simulations in the region of the SM and CEV was significant. The aft end of the SM was loaded by excessively large pressure–time histories, resulting in structural loads that would overwhelm the SM structure and result in significant loading of the aft end of the CEV. The conclusion to be drawn from these simulations is that if the CEV remains attached to the SM and second-stage booster and an explosive accident occurs of this type, the loading of the SM (and, subsequently, the CEV) is so severe that it would not be a survivable event for the crew.

Finally, a methodology was formulated and demonstrated that predicts the magnitude of key parameters descriptive of the explosive-hazard potential posed to the crew by a launch vehicle during ascent.

References

[1] Kinney, G. F., and Graham, K. J., *Explosive Shocks in Air*, Springer–Verlag, Berlin, 1985.

[2] Altmann, J., "Acoustic Weapons—A Prospective Assessment: Sources, Propagation, and Effects of Strong Sound," Cornell Univ. Paper 22, May 1999.

[3] McGlaun, J. M., Thompson, S. L., and Elrick, M. G., "CTH: A Three-Dimensional Shock Wave Physics Code," *International Journal of Impact Engineering*, Vol. 10, Nos. 1–4, 1990, pp. 351–360. doi:10.1016/0734-743X(90)90071-3

[4] Wilkins, M. L., *Computer Simulation of Dynamic Phenomena*, Springer–Verlag, Berlin, 1999.

[5] Joseph, C. J., and Freitas, C. J., "DD(X) PVLS Modeling and Simulation Verification and Validation Report," DD(X) PVLS EDM Design Team Report, Apr. 2005.

[6] Bunker-Farrah, R. L., Eck, M., Taylor, J. W., and Hancock, S., "Correlation of Liquid Propellants," NASA Johnson Space Center, White Sands Test Facility, Rept. WSTF-TR-0985-001-01-02, Los Cruces, NM, Sept. 2002.

[7] Gugan, K., *Unconfined Vapor Cloud Explosions*, Gulf, Houston, TX, 1979.

[8] Grady, D. E., "The Spall Strength of Condensed Matter," *Journal of the Mechanics and Physics of Solids*, Vol. 36, No. 3, 1988, pp. 353–384. doi:10.1016/0022-5096(88)90015-4

[9] Kipp, M. E., Grady, D. E., and Swegle, J. W., "Numerical and Experimental Studies of High-Velocity Impact Fragmentation," *International Journal of Impact Engineering*, Vol. 14, Nos. 1–4, 1993, pp. 427–438. doi:10.1016/0734-743X(93)90040-E

[10] Freitas, C. J., Keedy, R. M., and Sharron, T. R., "Crew Escape Risk Envelope Assessment," Southwest Research Inst., San Antonio, TX, Dec. 2005.

A. Ketsdever
Associate Editor